



Effect of Hydrothermal Reaction Time on Structural, Optical, and Catalytic Properties of Tin Oxide Nanoparticles

T. Preethi¹ · K. Senthil¹  · S. Ashokan¹  · R. Balakrishnaraja² · B. Sundaravel³

Received: 25 February 2021 / Accepted: 19 May 2021 / Published online: 4 June 2021
© Sociedade Brasileira de Física 2021

Abstract

The effect of hydrothermal reaction time on the structural, optical, and catalytic properties was investigated for the tin oxide (SnO₂) nanoparticles synthesized by employing a surfactant-free hydrothermal process. The formation of pure SnO₂ nanoparticles having tetragonal rutile structures was confirmed from the structural analysis using X-ray diffraction. The existence of direct relation between crystallinity and hydrothermal reaction time was evidenced from the observed higher crystallinity and larger crystalline size for the nanoparticles synthesized at longer hydrothermal reaction time. The morphological investigation using SEM analysis showed nanoparticles with nearly spherical shaped morphology with agglomeration. The optical analysis using UV–visible absorption spectra indicated slight blue shift in optical band gap energy values. Reduction in the intensity of visible emission PL band for the sample synthesized at longer hydrothermal reaction time further confirmed the formation of higher crystalline samples. H₂O₂-assisted catalytic degradation of crystal violet dye carried out under ambient conditions showed a maximum degradation efficiency for the sample synthesized at longer hydrothermal reaction time.

Keywords Metal oxides · SnO₂ nanoparticles · Hydrothermal method · Optical properties · Dye degradation

1 Introduction

Crystal violet dye was used as a model pollutant to study the catalytic degradation efficiency of metal oxides since it is mutagenic, unsafe, and carcinogenic in nature. A minimum concentration of < 1 ppm can have adverse effect on photosynthesis. Even inhalation of crystal violet dye can cause painful sensitization and horrible irritation due to its triphenylmethane structure. Although crystal violet dye is toxic to human health, plants, and aquatic life, it is produced and consumed in various fields including textile industry, biological staining, and dermatological agent in veterinary medicine. Hence, there is an emerging need to treat it properly before discharging it into the environment. Numerous

techniques are available for removing the organic pollutants in aqueous medium including precipitation, electrochemical, coagulation and flocculation, and adsorption [1, 2]. Since these methods are quite expensive and produce secondary pollutants, advanced oxidation processes (AOP) act as a suitable alternative technique for the degradation of organic dyes from waste water. AOP offers efficient results due to the powerful generation of hydroxyl radical with low cost and environmental benignity. Various iron free catalysts such as copper oxide, manganese oxide, magnesium oxide, zinc oxide, and graphene oxide-based materials were used to activate H₂O₂ into reactive oxygen radicals for the degradation of organic pollutants [3–8].

Extensive research reports were available on degradation of toxic dyes by semiconductor metal oxide nanoparticles or composites using advanced oxidation processes. Among them, SnO₂ nanoparticles are found to be very promising due to their unique properties such as high surface reactivity, presence of more active sites, and high absorption power of light radiation [9]. It is well known that the reaction parameters such as reaction time, temperature, pH of the solution, pressure, solvent, and the addition of surfactant/capping agent have shown strong influence on the structural, optical, and chemical properties of the nanoparticles. Zhang

✉ K. Senthil
ksenthiludt@gmail.com

¹ Advanced Materials Research Laboratory, Department of Physics, Bannari Amman Institute of Technology, 638 401, Sathyamangalam, TN, India

² Department of Food Technology, Bannari Amman Institute of Technology, 638 401, Sathyamangalam, TN, India

³ Materials Science Group, Indira Gandhi Centre for Atomic Research, HBNI, 603 102, Kalpakkam, TN, India

et al. have reported the formation of spherical and flower like nanoparticles on varying the hydrothermal reaction time and flower-like nanoparticles exhibited excellent sensing performance towards the ethanol gas [10]. Liu et al. proposed the optimized synthesis conditions such as reaction time and temperature during the hydrothermal process to produce urchin like SnO₂ nanocatalysts and reported the exhibition of significant improvement in electrochemical reduction of CO₂ by the synthesized nanocatalysts [11]. The influence of hydrothermal reaction time on the surface morphology of the SnO₂ nanostructures was investigated by Arote et al. [12]. It was reported that the reaction time significantly influenced the morphology with the formation of nanoflowers with self-assembled SnO₂ nanopetals showing enhanced photovoltaic performance. Thus, it was expected that hydrothermal reaction time will greatly influence the structural, optical, and catalytic properties of SnO₂ nanostructures. In the present work, we have studied the effect of hydrothermal reaction time on the structural, morphological, optical, and catalytic dye degradation properties of SnO₂ nanoparticles. The fast recombination rate of electron–hole pairs in most of the catalytic nanomaterials retards the efficiency of dye degradation, and it has been shown that H₂O₂-assisted catalytic degradation process can reduce the electron–hole pair recombination rate for enhanced catalytic efficiency [13]. Hence, we have adopted H₂O₂-assisted catalytic degradation process to investigate the degradation efficiency of synthesized SnO₂ nanoparticles towards crystal violet dye.

2 Experimental Procedures

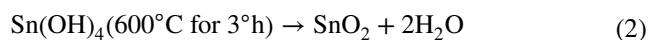
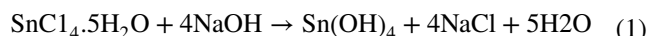
2.1 Materials

For the synthesis of SnO₂ nanoparticles, the following chemicals, tin (IV) chloride pentahydrate (SnCl₄·5H₂O), sodium hydroxide (NaOH), and methanol (CH₃OH), were used. All the chemicals were used as received without any further purification. Double distilled water was used as a solvent.

2.2 Synthesis of SnO₂ Nanoparticles

An aqueous solution of tin chloride was obtained by dissolving 7.012 g SnCl₄·5H₂O in 50 ml of double-distilled water. In order to adjust the pH value close to 10, NaOH solution was added drop-wise into the above solution under continuous stirring. The solution was stirred for about 30 min at room temperature after the solution became milky white in color. The milky white suspension was then transferred into a Teflon lined stainless steel autoclave and subjected to hydrothermal process at 150 °C for different reaction times 6 h, 12 h, and 18 h. After the completion of reaction, the autoclave cooled naturally and reached the room temperature.

The resultant precipitate was obtained by centrifuging and washing several times with distilled water and methanol to remove the unreacted impurities. The final products were dried at 80 °C for 12 h and calcined at 600 °C for 3 h. The reaction mechanism for the synthesis of SnO₂ nanoparticles is explained based on the following reactions [14]



When tin chloride reacts with NaOH, the Cl[−] ions surrounding the Sn atoms will be replaced by OH[−] ions to form tin (IV) hydroxide and NaCl. The produced NaCl will be removed after several washing. Finally, the SnO₂ nanoparticles can be obtained after the annealing process.

2.3 Characterization Techniques

The X-ray diffraction measurements were carried out using XPERT PRO diffractometer with CuKα radiation (λ = 1.54Å). The optical properties such as optical absorbance and photoluminescence were studied using UV–visible absorption spectrometer (JASCO UV V-770) and photoluminescence spectrometer (JASCO FP-8300) with an excitation wavelength of 250 nm and Xenon lamp as the light source, respectively. The surface morphology of the nanoparticles was analyzed using a scanning electron microscope (VEGA3 TESCAN). Degradation efficiency of the synthesized SnO₂ nanoparticles was investigated by observing the degradation of crystal violet dye in the presence of H₂O₂ at room temperature under normal light conditions, and the measurements were carried out using a UV–visible spectrophotometer (SCHIMADZU UV-1800).

3 Results and Discussion

3.1 X-Ray Diffraction Analysis

X-ray diffraction patterns of SnO₂ nanoparticles synthesized at different reaction times were shown in Fig. 1. The peaks observed at 26.56°, 33.92°, 37.82°, 51.79°, 54.84°, 57.98°, 61.86°, 65.33°, 71.26°, and 78.85° correspond to diffraction peaks obtained from the crystalline planes (110), (101), (200), (211), (220), (002), (310), (301), (202), and (321) respectively. These results were in accordance with the standard JCPDS data no. 41-1445 and confirmed the formation of tetragonal crystal system with P42/mnm space group. Any other peaks related to the impurity or secondary phases were not observed in the spectra. On observing these XRD patterns, it has been noted that the intensity of the peak increases with increase in reaction time and the

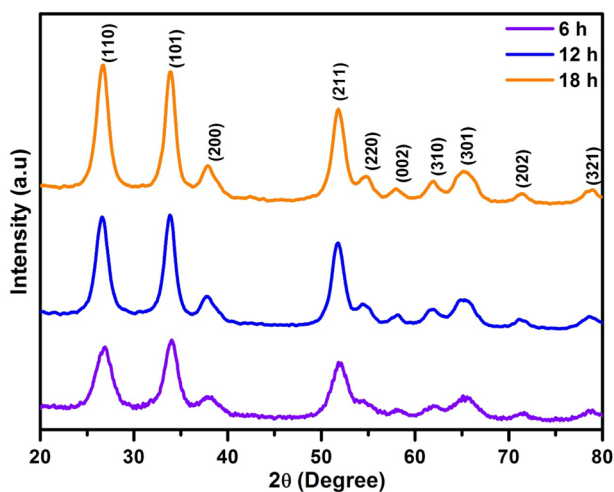


Fig. 1 XRD patterns of SnO₂ nanoparticles synthesized at different hydrothermal reaction times

sample synthesized at 18 h showed sharp and intense peaks indicating good crystalline nature. A similar observation of increasing intensity with increase in duration of hydrothermal reaction was reported earlier by Akhir et al. for tin oxide nanostructures [15]. The average crystallite size of the nanoparticles was calculated from Debye–Scherrer’s formula, whereas the dislocation density and micro-strain values were obtained from the Williamson and Small man’s formula. The calculated values of crystalline size, dislocation density, and micro-strain were given in Table 1. The minimum dislocation density and micro-strain values were obtained for the SnO₂ nanoparticles synthesized at a longer hydrothermal reaction time of 18 h. The values listed in the Table 1 clearly indicate increase of crystallinity of the samples with the increase of hydrothermal reaction time. During longer hydrothermal reaction time, the particles will have increased contact time with each other favoring greater coalescence and also have sufficient time to control the nanocrystal growth. Thus, the observed results confirmed the evidence of direct relation between the crystallinity and the duration of hydrothermal reaction.

Table 1 Structural parameters of SnO₂ nanoparticles calculated from the XRD patterns

Reaction duration (h)	Crystalline size (nm)	Dislocation density (lines/m ²)	Micro-strain
6	4.47	0.050	0.7123
12	4.68	0.045	0.4486
18	5.85	0.029	0.3575

3.2 Surface Morphology

The surface morphology of the nanoparticles synthesized at different hydrothermal reaction times (12 and 18 h) analyzed using SEM micrographs were shown in Fig. 2a, b. The SEM micrograph (Fig. 2b) obtained for the nanoparticles synthesized at longer hydrothermal reaction time clearly indicated the formation of nearly spherical shaped nanoparticles with agglomeration of particles. At longer reaction time (18 h), the particles were uniform and larger in size when compared to the shorter reaction time (12 h). At shorter duration, the agglomeration of particles tends to be more.

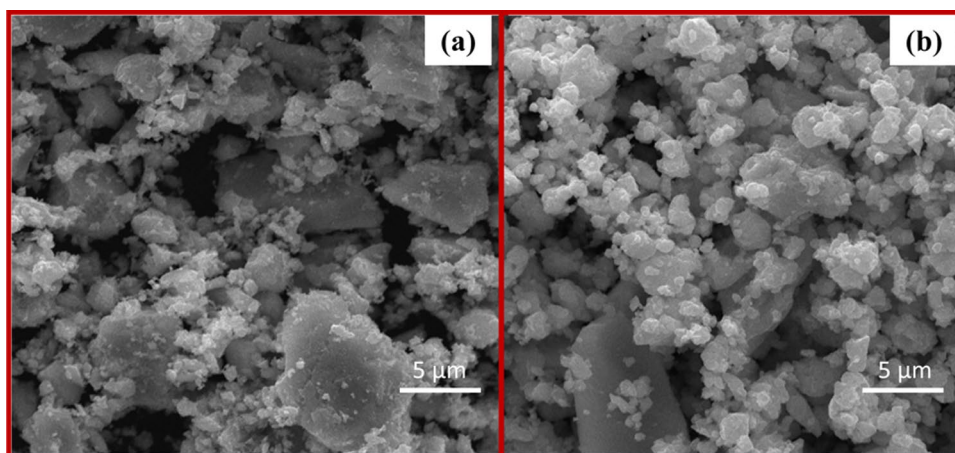
3.3 UV-Visible Absorption Spectroscopy

The UV–visible absorption spectra of SnO₂ nanoparticles recorded in the range 200–800 nm were shown in Fig. 3. It was found that the synthesized nanoparticles absorb mainly in the UV region due to the wide band gap of SnO₂. Similar absorption spectra were observed for the SnO₂ nanomaterials synthesized via sol–gel method [16] and also using electrochemically active biofilm [17]. The absorption band edges were found to have slight red shift with increasing reaction time resulting in the decrease of band gap energy values. The band gap energy of the synthesized nanoparticles can be calculated by using Tauc-Lorentz relation [18]

$$(\alpha h\nu) = B(h\nu - E_g)^n \quad (3)$$

where α is the absorption coefficient and $h\nu$ is the photon energy and n is a constant which depends on the nature of electronic transitions. SnO₂ is a direct band gap material; hence, we have chosen $n = 1/2$. The band gap can be obtained by extrapolating the linear portion of $(\alpha h\nu)^2$ on energy axis ($h\nu$) shown in the inset of Fig. 3. In general, the band gap of nanoparticle depends largely on crystal size, morphology, and specific surface area [19]. The band gap values of SnO₂ nanoparticles synthesized at different reaction time were found to be 2.85 eV (6 h), 2.76 eV (12 h), and 2.69 eV (18 h). The blue shift in band gap energy values observed with the increase in reaction time may be due to increase in crystallinity. Improvement in crystalline quality ultimately leads to decrease of defects present in the SnO₂ nanoparticles. It is prominent that the defects present in SnO₂ nanoparticles can form Fermi level inside the conduction band and leads to the increase in band gap. Hence, the observed decrease in band gap energy indicates the reduction of defects present inside the SnO₂ lattice [20]. This result was further confirmed from the crystalline size, dislocation density, and micro-strain values calculated from the XRD analysis.

Fig. 2 SEM micrographs of SnO₂ nanoparticles synthesized at different hydrothermal reaction times (a) 12 h and (b) 18 h



3.4 Photoluminescence Spectroscopy

The room temperature photoluminescence spectra recorded in the range between 270 and 700 nm with an excitation wavelength of 250 nm were depicted in Fig. 4. A sharp UV emission peak at ~ 291 nm and broad emission band in the visible region was observed. The UV emission was attributed due to near band edge emission, whereas the broad visible emission peak was due to transition of electrons from defect states such as oxygen vacancies present in the material [21]. The emission peak obtained at ~ 291 nm showed a red shift on increasing reaction time. This shift in peak position can be related to the variation in size of the particles. The reduction in intensity of visible emission peak indicates the presence of fewer defects which is consistent with the results obtained from X-ray analysis and UV–visible absorption spectra. The observed minimum PL intensity for the sample synthesized under longer reaction time indicates that the electron hole pair recombination rate was slow which could be more favorable for the dye degradation process.

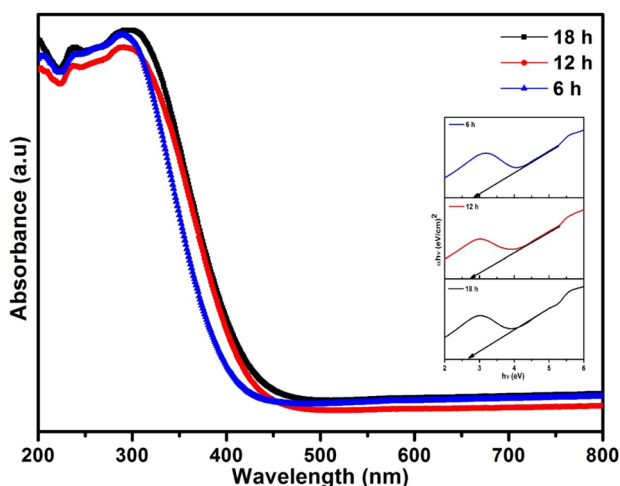


Fig. 3 UV–visible absorption spectra and Tauc's plot of SnO₂ nanoparticles synthesized at different hydrothermal reaction times

3.5 Catalytic Dye Degradation

The catalytic degradation of crystal violet dye was carried out for the SnO₂ nanoparticles using H₂O₂-assisted advanced oxidation process. The dye degradation experiment was performed under normal daylight conditions without the aid of any focused light sources to initiate the reaction. Initially, a dye solution was prepared for the required ppm, and then, the specific dose of catalyst

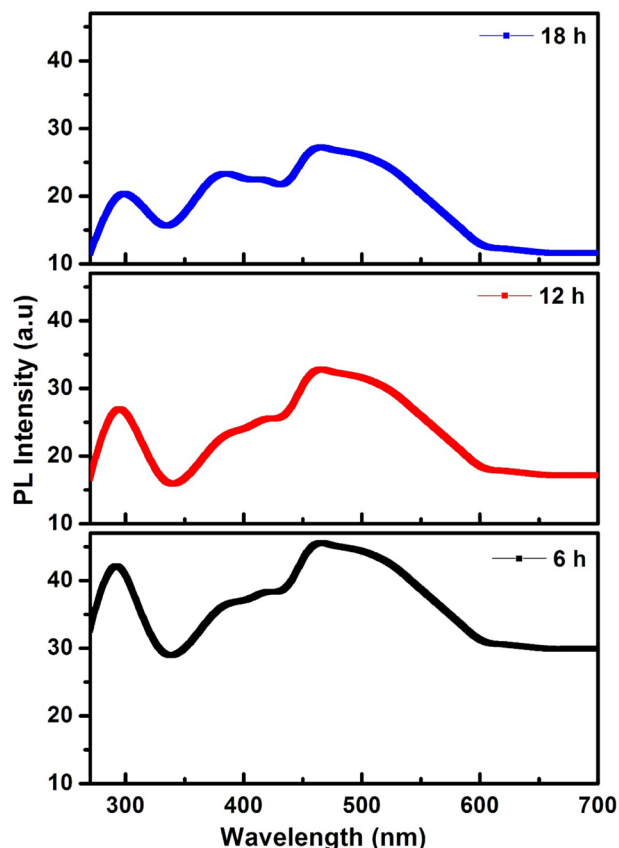


Fig. 4 PL spectra of SnO₂ nanoparticles synthesized at different hydrothermal reaction times

material (20 mg) was added to the dye solution and stirred continuously at room temperature. An appropriate amount of H_2O_2 (0.5 ml) is added to the dye solution under continuous stirring to initiate the catalytic reaction. At regular intervals of time, 4 ml of the solution is taken to determine the concentration of the dye solution using a UV–visible spectrophotometer.

Figure 5a–c shows the UV–visible absorption spectra of crystal violet dye solution at regular intervals during the catalytic degradation using SnO_2 nanoparticles synthesized under different reaction time 6, 12, and 18 h, respectively. It is found that the characteristic absorption band of crystal violet dye at 590 nm gradually decreased with increasing time with a change in color of the dye, indicating the chromophoric decomposition of the dye. The degradation time decreases on increasing the hydrothermal reaction time and the dye solution became colourless within 10 min for sample synthesized at 18 h hydrothermal reaction. This can be attributed due to the retardation of electron

hole recombination rate, and the same was evidenced from photoluminescence spectra. The possible degradation mechanism can be simply explained by a Fenton-like catalytic process. When the catalyst material is added to the dye solution, the catalyst material will be adsorbed on the organic dye molecules. When H_2O_2 is added into the crystal violet dye solution, hydroxyl radicals (OH^\cdot) will be formed due to the catalytic reaction of SnO_2 nanoparticles at the liquid–solid interface. The generated OH radicals degrade the dye solution, resulting in oxidation, and the degradation reaction will take place until the H_2O_2 is exhausted. A similar Fenton-like catalytic process has been reported for the degradation of Rhodamine B using free standing and flexible Cu@CuO nanowires [3]. The degradation efficiency is calculated by using the relation.

$$\text{Degradation Efficiency} = \left[1 - \frac{A}{A_0} \right] \times 100$$

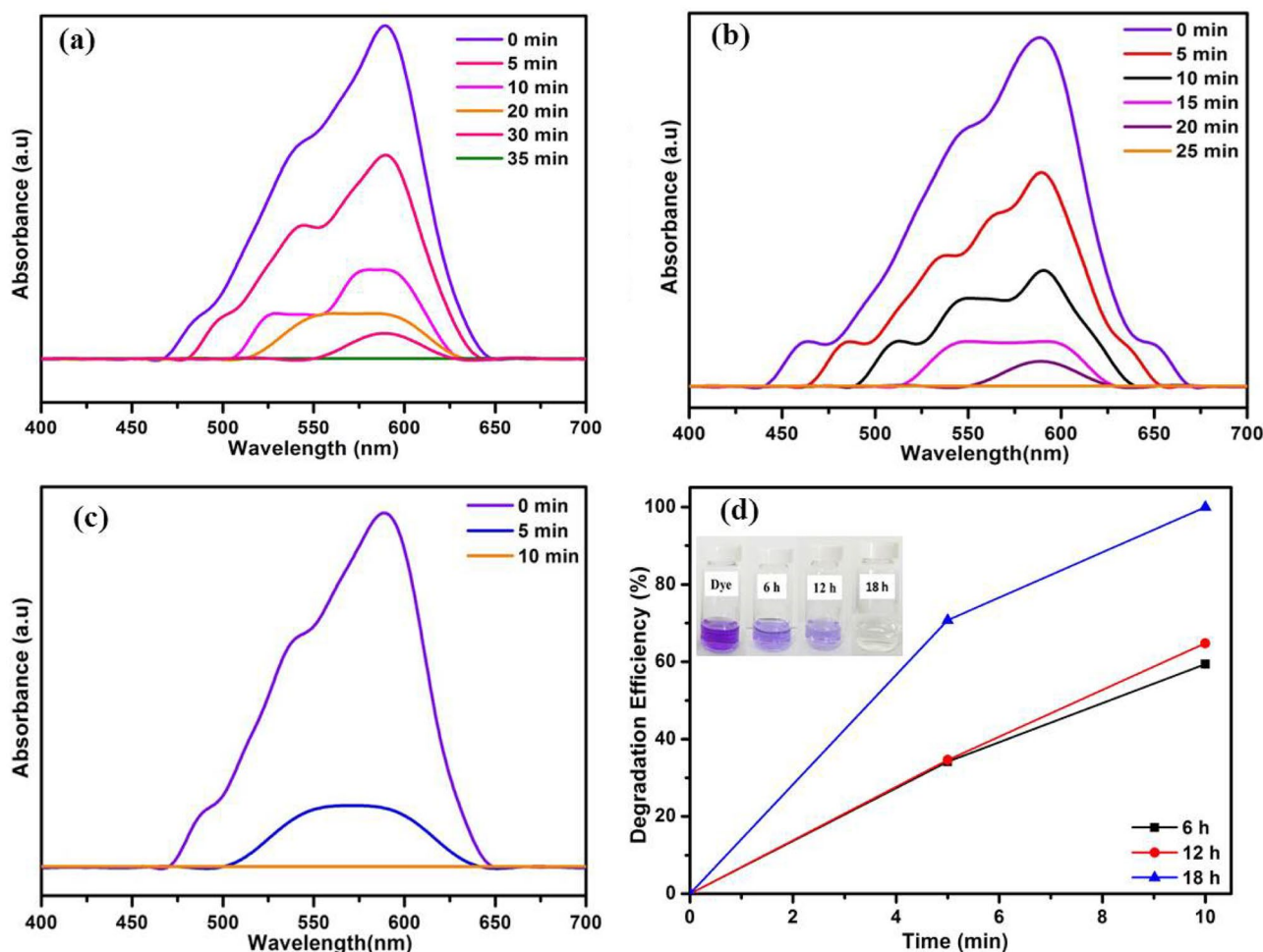


Fig. 5 Degradation of crystal violet dye using SnO_2 nanoparticles synthesized at different hydrothermal reaction times (a) 6 h, (b) 12 h, and (c) 18 h, and (d) dye degradation efficiency

where A_0 is the initial absorbance of the dye solution and A is the absorbance of the dye solution after catalytic degradation at regular intervals of time. The degradation efficiency of the SnO₂ nanoparticle catalyst with time for different hydrothermal reaction time was shown in Fig. 5d. A maximum degradation efficiency of 100% was observed for the SnO₂ nanoparticles synthesized at longer hydrothermal reaction time.

4 Conclusion

In summary, we have studied the effect of varying the duration of hydrothermal reaction on synthesis of SnO₂ nanoparticles without using any surfactant. XRD patterns confirmed the formation of tetragonal rutile structure with high crystalline quality for the SnO₂ nanoparticles synthesized at 18 h. SEM micrographs indicated that the size of the nanoparticles increased with increase in hydrothermal reaction time and seems to be uniform at longer reaction time. The formation of defect-less nanoparticles was confirmed from the XRD, UV, and PL analyses for the sample synthesized at longer hydrothermal reaction time. The nanoparticles synthesized at 18 h showed complete degradation of crystal violet dye for minimum dosage of catalyst (20 mg) in 10 min under normal light conditions.

Funding This work is financially supported by UGC-DAE-Consortium for Scientific Research (Project Sanction No. CSR-KN/CRS-107/2018–19/1046).

Declarations

Competing Interests The authors declare no competing interests.

References

1. S. Gautam, H. Agrawal, M. Thakur, A. Akbari, H. Sharda, R. Kaur, M. Amini, Metal oxides and metal organic frameworks for the photocatalytic degradation: a review. *J. Environ. Chem. Eng.* **8**(3), 103726 (2020)
2. R. Aggarwal, D. Saini, B. Singh, J. Kaushik, A.K. Garg, S.K. Sonkar, Bitter apple peel derived photoactive carbon dots for the sunlight induced photocatalytic degradation of crystal violet dye. *Sol. Energy.* **197**, 326–331 (2020)
3. Z. Su, J. Li, D. Zhang, P. Ye, H. Li, Y. Yan, Novel flexible Fenton-like catalyst: unique CuO nanowires arrays on copper mesh with high efficiency across a wide pH range. *Sci. Total Environ.* **647**, 587–596 (2019)
4. Y. Zhang, C. Liu, B. Xu, F. Qi, W. Chu, Degradation of benzotriazole by a novel Fenton-like reaction with mesoporous Cu/MnO₂: combination of adsorption and catalysis oxidation. *Appl. Catal. B.* **199**, 447–457 (2016)
5. D. Wu, Y. Bai, W. Wang, H. Xia, F. Tan, S. Zhang, B. Su, X. Wang, X. Qiao, P.K. Wong, Highly pure MgO₂ nanoparticles as robust solid oxidant for enhanced Fenton-like degradation of organic contaminants. *J. Hazard. Mater.* **374**, 319–328 (2019)
6. Md.T. Uddin, Md.E. Hoque, M.C. Bhoumick, Facile one-pot synthesis of heterostructure SnO₂/ZnO photocatalyst for enhanced photocatalytic degradation of organic dye. *RSC. Adv.* **10**, 23554–23565 (2020)
7. S.E.G.D. Rani, A.G. Kumar, S. Steplinpaulselvin, R. Rajaram, T.S. Silambarasan, I.S. Lydia, Y. Chen, Survival assessment of simple food webs for dye wastewater after photocatalytic degradation using SnO₂/GO nanocomposites under sunlight irradiation. *Sci. Total Environ.* **721**, 137805 (2020)
8. L. Zhang, D. Xu, C. Hu, Y. Shi, Framework Cu-doped AlPO₄ as an effective Fenton-like catalyst for bisphenol A degradation. *Appl. Catal. B.* **207**, 9–16 (2017)
9. A. Bhattacharjee, Md. Ahmaruzzaman, T. Sinha, Surfactant effects on the synthesis of durable tin-oxide nanoparticles and its exploitation as a recyclable catalyst for elimination of toxic dye: a green and efficient approach for wastewater treatment. *RSC Adv.* **4**, 51418–51429 (2014)
10. H. Zhang, W. Zeng, Y. Li, B. Miao, W. Chen, Synthesis of SnO₂ flower-like architectures by varying the hydrothermal reaction time. *J. Mat. Sci.: Mat. Electron.* **25**, 3674–3679 (2014)
11. Y. Liu, M. Fan, X. Zhang, Q. Zhang, D. Guay, J. Qiao, Design and engineering of urchin-like nanostructured SnO₂ catalysts via controlled facile hydrothermal synthesis for efficient electro-reduction of CO₂. *Electrochim. Acta.* **248**, 123–132 (2017)
12. S.A. Arote, V.A. Tabhane, H.M. Pathan, Enhanced photocatalytic performance of dye sensitized solar cell using SnO₂ nano-flowers. *Opt. Mater.* **75**, 601–606 (2018)
13. X. Rong, F. Qiu, J. Rong, X. Zhu, J. Yan, D. Yang, Enhanced visible light photocatalytic activity of W-doped porous g-C₃N₄ and effect of H₂O₂. *Mater. Lett.* **164**, 127–131 (2016)
14. M.U. Khalid, S.R. Khan, S. Jamil, Morphologically controlled synthesis of cubes like tin oxide nanoparticles and study of its application as photocatalyst for Congo red degradation and as fuel additive. *J. Inorg. Organomet. Polym.* **28**, 168–176 (2018)
15. M.A.M. Akhbar, K. Mohamed, H.L. Lee, S.A. Rezan, Synthesis of tin oxide nanostructures using hydrothermal method and optimization of its crystal size by using statistical design of experiment. *Procedia Chem.* **19**, 993–998 (2016)
16. S. Arya, M. Riyas, A. Sharma, B. Singh, Prerna, P. Bandhoria, S. Khan, V. Bharti, Electrochemical detection of ammonia solution using tin oxide nanoparticles synthesized via sol-gel route. *Appl. Phys. A.* **124**, 538 (2018)
17. S.A. Ansari, M.M. Khan, M.O. Ansari, J. Lee, M.H. Cho, Visible light-driven photocatalytic and photoelectrochemical studies of Ag-SnO₂ nanocomposites synthesized using an electrochemically active biofilm. *RSC Adv.* **4**, 26013–26021 (2014)
18. H. Letifi, Y. Litaïem, D. Dridi, S. Ammar, R. Chtourou, Enhanced photocatalytic activity of vanadium-doped SnO₂ nanoparticles in rhodamine B degradation. *Adv. Condens. Matter Phys.* **2019**, 2157428 (2019)
19. M. Wang, Y. Gao, Z. Chen, C. Cao, J. Zhou, L. Dai, X. Guo, Transparent and conductive W-doped SnO₂ thin films fabricated by an aqueous solution process. *Thin Solid Films* **544**, 419–426 (2013)
20. R. Ahmad, N. Afzal, U. Amjad, S. Jabbar, T. Hussain, A. Hussain, Structural and optical properties of DC magnetron sputtered ZnO films on glass substrate and their modification by Ag ions implantation. *Mater. Res. Express.* **4**, 076411 (2017)
21. D.M. Priyadarshini, R. Mannam, M.S.R. Rao, N.D. Gupta, Effect of annealing ambient on SnO₂ thin film transistors. *Appl. Surf. Sci.* **418**, 414–417 (2016)

Publisher's Note Springer Nature remains neutral with regard to jurisdictional claims in published maps and institutional affiliations.